Compressing neural network by tensor network with exponentially fewer variational parameters

Yong Qing*,[1] Ke Li*,[1] Peng-Fei Zhou,[1] and Shi-Ju Ran[1, *]

[1]*Center for Quantum Physics and Intelligent Sciences,*
Department of Physics, Capital Normal University, Beijing 10048, China
(Dated: May 6, 2024)

Neural network (NN) designed for challenging machine learning tasks is in general a highly nonlinear mapping that contains massive variational parameters. High complexity of NN, if unbounded or unconstrained, might unpredictably cause severe issues including over-fitting, loss of generalization power, and unbearable cost of hardware. In this work, we propose a general compression scheme that significantly reduces the variational parameters of NN by encoding them to deep automatically-differentiable tensor network (ADTN) that contains exponentially-fewer free parameters. Superior compression performance of our scheme is demonstrated on several widely-recognized NN's (FC-2, LeNet-5, AlextNet, ZFNet and VGG-16) and datasets (MNIST, CIFAR-10 and CIFAR-100). For instance, we compress two linear layers in VGG-16 with approximately 10^7 parameters to two ADTN's with just 424 parameters, where the testing accuracy on CIFAR-10 is improved from 90.17% to 91.74%. Our work suggests TN as an exceptionally efficient mathematical structure for representing the variational parameters of NN's, which exhibits superior compressibility over the commonly-used matrices and multi-way arrays.

I. INTRODUCTION

Neural network (NN) [1] has gained astounding success in a wide range of fields including computer vision, natural language processing, and most recently scientific investigations in, e.g., applied mathematics(e.g., [2, 3]) and physics(e.g., [4–10]). To improve the performance on handling complicated realistic tasks, the amount of variational parameters in NN rapidly increases from millions to trillions (e.g., Chat-GPT with 175 billion parameters [11]). Such a paradigm with the utilization of super large-scale NN's brought us several severe challenges. Though the representation ability of NN should be enhanced by increasing the complexity, over-fitting might occur and the generalization ability of NN might unpredictably be harmed. The increasing complexity also brings unbearable cost of hardware in academic investigations and practical applications.

The variational parameters in NN are usually stored as matrices or higher-order tensors (also called multi-linear arrays). Previous results show that generalization ability can be improved by suppressing or "refining" the degrees of freedom in such tensors by, e.g., network pruning [12–14], knowledge distillation [15, 16], weight sharing [17, 18], tensor decompositions [19, 20], etc. In recent years, shallow tensor networks (TN's) including matrix product state (MPS [21, 22], also known as tensor-train form [23]) and matrix product operator (MPO [24]) were applied to represent the tensors in neural networks, and achieved remarkable compression rates [25–29]. These imply TN as a superior mathematical structure over the simple multi-linear arrays for representing the variational parameters of NN's, which yet remains an open issue.

In this work, we propose to encode the variational parameters of the considered NN layer(s) into the contraction of TN [30] that contains exponentially fewer parameters. See the illustration of the main procedures in Fig. 1. For instance,
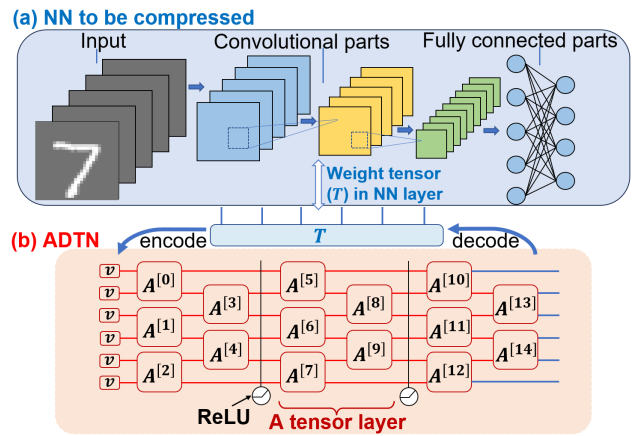
FIG. 1. (Color online) The workflow of ADTN for compressing NN. (a) The illustration of a convolutional NN as an example, whose variational parameters (T) are encoded in a ADTN shown in (b). The contraction of the ADTN results in T, in other words, where the ADTN contains much less parameters than T.

the number of parameters of the TN encoding 2^Q parameters of NN scale just linearly as $O(MQ)$, with $M \sim O(1)$ the number of TN layers. Since the contraction process is differentiable, automatic differentiation technique [31, 32] is utilized to optimize the tensors of the TN to reach the optimal accuracy after compression. Thus, we dub our scheme as automatically differentiable tensor network (ADTN).

We demonstrate the compression performance of ADTN on various well-known NN's (FC-2, LeNet-5 [33], AlexNet, ZFnet, and VGG-16 [34]) and datasets (MNIST [35], CIFAR-10 [36] and CIFAR-100). Note the details of NN's can be found in Appendix A. For instance, in the experiment of compressing two fully connected layers of VGG-16, we compressed about 10^7 parameters to two ADTN's with just 424, where the accuracy of the testing set of CIFAR-10 is improved from 90.17% to 91.74%. Our work implies a general way to reduce the excessive complexity of NN's by encoding the

variational parameter into TN as a more compact and efficient mathematical form.

II. METHOD

A NN can be formally written as a mapping

$$\boldsymbol{y} = f(\boldsymbol{x}; \boldsymbol{T}, \boldsymbol{T}', \ldots), \tag{1}$$

which maps the input sample $\boldsymbol{x}$ to the output vector $\boldsymbol{y}$. We aim to compress the variational parameters $(\boldsymbol{T}, \boldsymbol{T}', \ldots)$ or a part of them by ADTN. Note we do not assume the types of layers (linear, convolutional, etc.) in the NN as it makes no difference to our ADTN method.

Denoting the parameters to be compressed as tensor $\boldsymbol{T}$, our idea is to represent $\boldsymbol{T}$ as the contraction of ADTN with multiple layers. The structure of ADTN is flexible. Here, we choose the commonly-used "brick-wall" structure; see an example of its diagrammatic representation in Fig. 1 (b). In simple words about the diagrammatic representation of TN, each block represents a tensor, and the bonds connected to a block represent the indexes of the corresponding tensor. Shared bonds represent the dumb indexes that should be summed up (contracted). The vertical black lines represent the activation function (e.g., ReLU). More details about TN contractions and the diagrammatic representation can be found in Appendix A or Ref. [30].

For simplicity, we assume to compress 2^Q variational parameters, i.e., $\#(\boldsymbol{T}) = 2^Q$, into one ADTN. Obviously, the contraction of ADTN should also give us a tensor (denoted as $\mathcal{T}$) containing 2^Q parameters. In our example, the ADTN results in a Q-th order tensor, where the dimension of each index is taken as $d = 2$. These indexes are represented by the unshared bonds in the ADTN. See the blue bonds on the right boundary of the diagrammatic representation in Fig. 1 (b).

The exemplified ADTN is formed by several $(d \times d \times d \times d)$ tensors $\{\boldsymbol{A}^{[k]}\}$ ($k = 0, \ldots, K-1$ with K their total number), which form the variational parameters of ADTN. On the left boundary of ADTN, we put several two-dimensional constant vectors $\boldsymbol{v}$ for the convenience in formulating and analyzing. We may take $\boldsymbol{v} = [1, 0]$ for instance.

For the brick-wall structure, we define each $(Q-1)$ tensors in two neighboring columns as a TN layer [depicted in Fig. 1 (b)]. We put an activation function between each two neighboring TN layers. Contracting the tensors in one tensor layer essentially gives us a $(2^Q \times 2^Q)$ matrix denoted as $\mathcal{L}^{(m)}$ for the m-th tensor layer. The mapping represented by the whole ADTN can be written as

$$\mathcal{T} = \mathcal{L}^{(M)} \sigma(\ldots \mathcal{L}^{(3)} \sigma(\mathcal{L}^{(2)} \sigma(\mathcal{L}^{(1)} \prod_{\otimes q=1}^{Q} \boldsymbol{v}))), \tag{2}$$

with $\otimes$ the tensor product and σ the activation function. In other words, $\mathcal{T}$ is obtained by implementing the mappings $\{\sigma(\mathcal{L}^{(m)}(*))\}$ (for $m = 1, 2, \cdots, M$ with M the number of TN layers) on $\prod_{\otimes q=1}^{Q} \boldsymbol{v}$. Be aware that one does not have to

simulate the matrices $\{\mathcal{L}^{(m)}\}$, which are introduced here only for the convenience of understanding and expressing. The total number of variational parameters in such a brick-wall ADTN scales as

$$\#(\text{ADTN}) \equiv \sum_k \#(\boldsymbol{A}^{[k]}) \sim O(MQ), \tag{3}$$

with $M \sim O(1)$ according to our results provided below. In plain words, we lower the exponential complexity $O(2^Q)$ to linear complexity $O(MQ)$ with respect to Q.

There are two main stages to obtain the tensors in ADTN $\{\boldsymbol{A}^{[k]}\}$. The first is pre-training by minimizing the distance between $\boldsymbol{T}$ and $\mathcal{T}$. We choose the loss function as Euclidean distance $L^{\text{E}} = |\mathcal{T} - \boldsymbol{T}|$. After L^{E} converges, we move to the second stage to minimize the loss function for implementing the machine learning task. One may choose the same loss function as the one used for training the NN, such as the cross entropy from the outputs of NN and the ground-truth classifications of the training samples. The feed-forward process of getting the output of the NN is the same as that for training the NN, except that the parameters ($\boldsymbol{T}$) of the target NN layer are replaced by the tensor ($\mathcal{T}$) obtained by contracting the ADTN. Generally speaking, the first stage is to enhance the stability by finding a proper initialization of ADTN, and the second stage further improves the performance with an end-to-end optimization. The mapping given by the NN in the second stage can be written as

$$\boldsymbol{y} = f(\boldsymbol{x}; \{\boldsymbol{A}^{[k]}\}, \boldsymbol{T}^{\text{res}}), \tag{4}$$

with $\boldsymbol{T}^{\text{res}}$ denoting the uncompressed parameters.

The number of compressed NN layers and that of ADTN's are flexible. The mapping of the compressed NN can be written as $\boldsymbol{y} = f(\boldsymbol{x}; \{\boldsymbol{A}^{[k]}\}, \{\boldsymbol{B}^{[k]}\}, \cdots, \boldsymbol{T}^{\text{res}})$, with $\{\boldsymbol{A}^{[k]}\}, \{\boldsymbol{B}^{[k]}\}, \cdots$ denoting the tensors of multiple ADTN's. This allows more convenient treatment on the cases where the number of the parameters cannot be written as d^Q. For instance, (3×2^{10}) parameters in a NN layer can be compressed to a single ADTN with totally $Q = 11$ unshared indexes, where 10 of them are two-dimensional and 1 is three-dimensional. It can also be divided into two parts with 2^{11} and 2^{10} parameters, respectively, which are then compressed to two ADTN's with $Q = 11$ and 10, respectively. All unshared indexes in these two ADTN's can be two-dimensional.

III. COMPRESSION PERFORMANCE

In Table I, the green area shows the performance of ADTN with $M = 1$ to compress linear layers in various NN's. High compression ratios $\rho = \mathcal{P}/P$ (with P and $\mathcal{P}$ the numbers of parameters in the compressed NN layer(s) and in the ADTN(s), respectively) are achieved. Our first example is FC-2 formed by two linear layers, whose sizes are (784×256) and (256×10), respectively. We slice out 2^{17} parameters from the first linear layer and compress them in an ADTN with just 160 parameters. The testing accuracy on the MNIST

TABLE I. ADTN's performance on compressing the linear layers (green area) and convolutional layers (oriange area) of FC-2, LeNet-5, Alex Net, ZF Net, and VGG-16 for MNIST, CIFAR-10, and CIFAR-100 datasets. We show the number of parameters in the compressed NN layer(s) P, that of ADTN(s) $\mathcal{P}$, compression ratio $\rho = \mathcal{P}/P$, the number of ADTN(s) N, and testing accuracies before compression η_{NN} and after compression η. The hyper-parameters of these NN's can be found in Appendix B.

Dataset		NN Model	#Parameters		Compression ratio $\rho = \mathcal{P}/P$	#ADTN N	Testing accuracy		
			Compressed NN layer(s) P	ADTN(s) $\mathcal{P}$			η_{NN}	η	η/η_{NN}
Compress **linear** layer(s)	MNIST	FC-2	131072	160	1.2×10^{-3}	1	97.94%	97.81%	99.69%
		LeNet-5	8192	120	1.5×10^{-2}	1	99.15%	99.48%	100.36%
	CIFAR-10	LeNet-5	163804	300	1.8×10^{-3}	2	74.39%	75.27%	101.18%
		AlexNet	5242880	388	7.4×10^{-5}	2	81.13%	81.31%	100.22%
		ZFNet	6291456	404	6.4×10^{-5}	2	80.59%	81.03%	100.66%
		VGG-16	18874368	424	2.2×10^{-5}	2	90.17%	91.74%	101.74%
	CIFAR-100	LeNet-5	163804	300	1.8×10^{-3}	2	41.30%	42.60%	103.15%
		AlexNet	5242880	388	7.4×10^{-5}	2	49.80%	49.19%	98.78%
		ZFNet	6291456	404	6.4×10^{-5}	2	50.19%	50.36%	100.34%
Compress **conv** layer(s)	MNIST	LeNet-5	32768	140	4.2×10^{-3}	1	99.15%	99.52%	100.37%
	CIFAR-10	LeNet-5	8192	120	1.5×10^{-2}	1	74.39%	75.16%	101.04%
		AlexNet	1572864	364	2.9×10^{-4}	2	81.13%	81.09%	99.95%
		ZFNet	393216	324	8.2×10^{-4}	2	80.59%	81.63%	101.29%
		VGG-16	11796480	1820	1.5×10^{-4}	10	90.17%	91.09%	101.02%
	CIFAR-100	LeNet-5	8192	120	1.5×10^{-2}	1	41.30%	42.54%	103.00%
		AlexNet	1572864	364	2.9×10^{-4}	2	49.80%	50.15%	100.70%
		ZFNet	393216	324	8.2×10^{-4}	2	50.19%	50.88%	101.37%

dataset, which consisting of 60000 hand-written images of size (28×28) [35], remains almost unchanged after compression. In more complex convolutional NN's (LeNet-5, AlexNet, and ZFNet), we chose to compress all linear layers except for the output layer. This is because the number of parameters in the output layer is much smaller compared to other layers. For different datasets (MNIST, CIFAR-10, and CIFAR-100), we just accordingly alter the dimensions for the input and output of each NN, and keep other hyper-parameters unchanged. Note CIFAR-10 and CIFAR-100 contain totally 80 million everyday-life RGB images of size (32×32) [36]. The ADTN's with just hundreds of parameters manage to compress the linear layers whose numbers of parameters vary from $O(10^3)$ to $O(10^7)$, while the testing accuracy is not harmed by compression. Remarkably in compressing VGG-16, we use two ADTN's with in total 424 parameters to compress two linear layers with approximately 10^7 parameters (whose dimensions are (512×4096) and (4096×4096), respectively), and meanwhile are able to increase the testing accuracy from 90.17% to 91.74%.

The orange area in Table I shows excellent performance of ADTN to compress convolutional layers. For example, we compress the two largest convolutional layers in AlexNet and ZFNet (with about $O(10^6)$ and $O(10^5)$ parameters) that account for more than 80% of the total parameters in the corresponding NN. These parameters are compressed to the ADTN's consisting of just 324 parameters. For VGG-16, we choose to compress the five largest layers from the 13 convolutional layers. Each convolutional layer used two ADTN's to compress. The testing accuracy is improved from about 1 percentage.

We shall emphasize that many settings of our ADTN compression scheme are flexible, such as the choices of compressed NN layers, the number of ADTN's, and the hyper-parameters of each ADTN. The demonstrated results in this paper are obtained after slightly adjusting these quantities. Higher compression performance can generally be reached by further adjusting them.

One can consider to simultaneously compress multiple types of NN layers. In Table II, we show the performance of ADTN for simultaneously compressing linear and convolutional layers of VGG-16. We use a reduced version of VGG-16 (with smaller sizes of the NN layers and without data augmentation) for demonstration, with its testing accuracy $\eta_{\mathrm{NN}} = 81.14\%$. The red bars in the first column indicate the compressed layers, and their lengths illustrate the num-

TABLE II. (Color online) The performance of ADTN scheme with different numbers of tensor layers (M) to compress both the linear and convolutional layers of a reduced version of VGG-16 (with its testing accuracy $\eta_{\text{NN}} = 81.14\%$). In the first column, the red bars indicate the compressed layers and their lengths illustrate the numbers of parameters. The second and third columns show the training and testing accuracies ($\tilde{\eta}$ and η, respectively). The last column gives the total compression ratio ρ_{tot} [Eq. (5)].

Compressed layers (red)	M	$\tilde{\eta}$	η	η/η_{NN}	ρ	ρ_{tot}
Conv	1	99.87%	84.27%	103.86%	5.0×10^{-5}	
	3	100%	85.52%	105.40%	2.1×10^{-4}	0.435
	5	100%	85.71%	105.63%	3.7×10^{-4}	
Conv	1	99.99%	84.36%	103.97%	6.0×10^{-5}	
	3	100%	85.19%	105.00%	2.5×10^{-4}	0.279
	5	100%	85.68%	105.60%	4.4×10^{-4}	
Conv	1	98.83%	78.53%	99.78%	8.0×10^{-5}	
	3	99.93%	82.44%	101.60%	3.3×10^{-4}	0.135
	5	100%	82.79%	102.03%	5.9×10^{-4}	
Conv+linear	1	96.35%	65.93%	81.25%	1.0×10^{-4}	
	3	99.94%	77.73%	95.78%	4.2×10^{-4}	0.060
	5	100%	79.15%	97.55%	7.4×10^{-4}	
	7	100%	80.61%	99.35%	1.1×10^{-3}	
Conv+linear	3	75.78%	72.13%	88.90%	1.0×10^{-4}	
	5	78.13%	74.24%	91.50%	4.2×10^{-4}	0.008
	7	81.54%	77.61%	95.65%	7.4×10^{-4}	
	9	81.95%	78.59%	96.86%	1.1×10^{-3}	

bers of parameters. Here, each NN layer is compressed to one ADTN. Remarkable compression rations (ρ) are achieved.

In the last column, we show the total compression ratio

$$\rho_{\text{tot}} = \frac{\#(\text{ADTN}) + \#(\boldsymbol{T}^{\text{res}})}{\#(\text{NN})} \simeq \frac{\#(\boldsymbol{T}^{\text{res}})}{\#(\text{NN})}. \qquad (5)$$

The approximation holds since in general we have $\#(\text{ADTN}) \ll \#(\boldsymbol{T}^{\text{res}}) \ll \#(\text{NN})$. Therefore, ρ_{tot} can be significantly improved by simply compressing more NN layers to ADTN's. Our results suggest that for $\rho \lesssim 0.3$, shallow ADTN (say with $M = 1$ tensor layer) is sufficient for compressing the chosen parts of the NN. The training accuracy $\tilde{\eta}$ is almost 100%, meaning the representational ability of the shallow ADTN is sufficient. As ρ decreases by compressing more NN layers, $\tilde{\eta}$ also decreases. Deeper ADTN with better representational ability is required. As shown in the last row, the testing accuracy is improved from 72.13% to 78.95% by increasing M from 3 to 9 when compressing 12 layers in VGG-16. The total compression ratio is lowered to $\rho_{\text{tot}} \simeq 0.008$.

IV. DISCUSSIONS ON OVER-PARAMETRIZATION, COMPRESSION ORDER, AND FAITHFULNESS

Below, we further discuss on several critical issues about the ADTN compression scheme. First, we show that by properly increasing the number of ADTN's (N), the NN can be well compressed whether it is under-fitting or over-fitting. We take LeNet-5 as an example and alter the output dimension of the first linear layer s (i.e., the input dimension of the second linear layer) to change the parameter complexity of the NN.

Fig. 2 (a) shows the testing-accuracy ratio η/η_{NN} versus the inverse total compression ratio ρ_{tot}^{-1} for the CIFAR-10 dataset with s ranging from 32 to 1536.

The NN with a small s is difficult to compress even by ADTN. In this case, the model is under-fitting, resulting in small ρ_{tot}^{-1} and η/η_{NN} (see the symbols with relatively light colors). By increasing N, η/η_{NN} will fairly approach to 1. In comparison, for the over-fitting case with large s, the NN is shown to be compressible by ADTN, leading to large ρ_{tot}^{-1} and $\eta/\eta_{\text{NN}} > 1$, particularly when using multiple ADTN's for compression ($N > 1$). See the symbols with dark colors. The testing accuracy is increased by compression with $\eta/\eta_{\text{NN}} > 1$, implying that the generalization ability is improved. Generally speaking, our results suggest that compressing by multiple ADTN's will avoid significant decrease of the testing accuracy in the under-fitting cases, and enhance generalization ability in the over-fitting cases.

Considering compressing multiple layers in a NN, one will suffer from severe local-minima problem. Simultaneously compressing several NN layers will be unstable since the optimization can easily be trapped in different local minima when taking different initializations of the ADTN's. A stable way is to compress layer by layer. Specifically, we start from the compression of one layer by encoding it as ADTN(s). After this is done, we compress another layer by optimizing the ADTN(s), and simultaneously optimize the ADTN(s) of the formerly-compressed layer. For each time the optimization process converges, we consider to compress one more layer by optimizing the ADTN(s) of this layer and those of all optimized layers simultaneously. This requires to determine a compression order.

Below we show that the compression order should be "backward", meaning compressing from the layers closer to the output of NN to those nearer the input. Fig. 2 (b) shows the η/η_{NN} versus ρ^{-1} for the CIFAR-10 dataset by the reduced VGG-16. We compress 12 largest layers therein from the input to output (forward) and the other way around. Much better performance is achieved by the backward compression. This is essentially due to the interdependence among the compressions of different layers. An accurate compression of a NN layer should require accurate input from the former layers in the information propagation process. We conjecture the above observation to be held when using other compression means.

We expect a well-performed compression scheme to at least faithfully restore the generalization ability of the original NN, despite the NN itself is well trained or not. It means that the testing accuracy after compression will be mainly determined by the testing accuracy of the original NN. Fig. 3 shows the testing accuracies before and after compression (denoted as η_{NN} and η) for VGG-16 on the CIFAR-10 dataset. Different before-compression testing accuracies are obtained by changing the number of training samples. Our results show that the ADTN compression scheme faithfully restores the testing accuracies of the NN with slight improvements. We expect the ADTN scheme to be faithful for compressing other NN models.
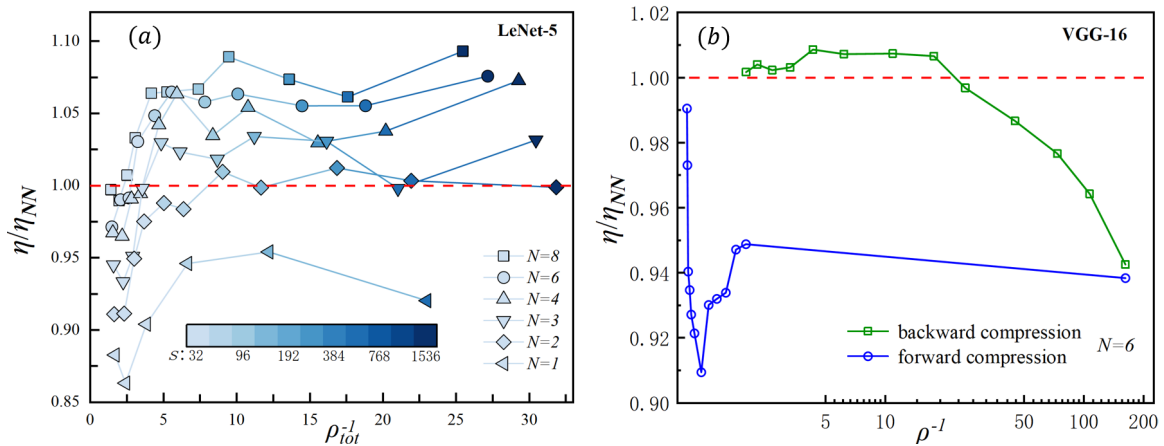
FIG. 2. (Color online) The testing-accuracy ratio $\eta/\eta_{\rm NN}$ versus the inverse total compression ratio $\rho_{\rm tot}^{-1}$ for the CIFAR-10 dataset by LeNet-5. The dimensions of the first two linear layers are taken as $(512 \times s)$ and $(s \times 128)$, where s is taken as $32, 64, \cdots, 1536$ (see the color bar). N ADTN's are used for compression, where each contains $M = 3$ tensor layers. The testing-accuracy ratio $\eta/\eta_{\rm NN}$ versus the inverse of compression ratio ρ^{-1} for the CIFAR-10 dataset by VGG-16. We selected 12 largest layers (ten convolutional and two linear layers) in VGG-16 and compress them in two different orders: from the input to output (denoted as forward compression) and the other way around (denoted as backward compression).
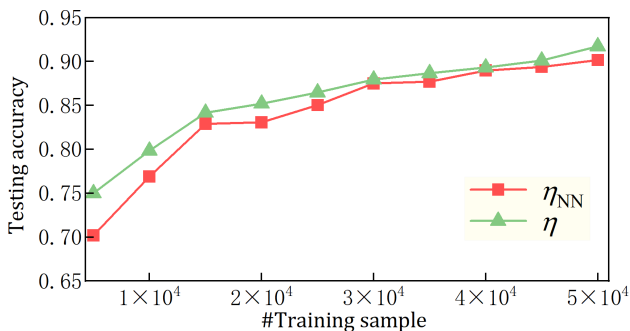

FIG. 3. (Color online) The testing accuracy of NN $\eta_{\rm NN}$ and that after compression η of VGG-16 on the CIFAR-10 dataset with different numbers of training samples. The compression by our ADTN scheme faithfully restores the testing accuracy of the original NN with slight improvements.

V. SUMMARY

In summary, we proposed a general compression scheme based on automatically differentiable tensor network (ADTN) to significantly reduce the variational parameters of neural networks (NN's). The key idea is to encode the higher-order parameter tensors of NN as the contractions of deep ADTN(s) that contain exponentially less parameters. The performance of our scheme has been demonstrated with several well-known NN's on different datasets. Discussions on over-parametrization, compression order, and faithfulness of our ADTN compression scheme are given. Our work suggests TN as a more efficient and compact mathematical form than the multi-way arrays to represent the variational parameters of NN's.

[1] Jürgen Schmidhuber. Deep learning in neural networks: An overview. *Neural Networks*, 61:85–117, 2015.

[2] Na Lei, Kehua Su, Li Cui, Shing-Tung Yau, and Xian-feng David Gu. A geometric view of optimal transportation and generative model. *Computer Aided Geometric Design*, 68:1–21, 2019.

[3] Alex Davies, Petar Veličković, Lars Buesing, Sam Black-well, Daniel Zheng, Nenad Tomašev, Richard Tanburn, Peter Battaglia, Charles Blundell, András Juhász, Marc Lackenby, Geordie Williamson, Demis Hassabis, and Pushmeet Kohli. Advancing mathematics by guiding human intuition with AI. *Nature*, 600(7887):70–74, 2021.

[4] Giuseppe Carleo and Matthias Troyer. Solving the quantum many-body problem with artificial neural networks. *Science*, 355(6325):602–606, 2017.

[5] Xun Gao and Lu-Ming Duan. Efficient representation of quantum many-body states with deep neural networks. *Nature Communications*, 8(1):662, 2017.

[6] Juan Carrasquilla and Roger G. Melko. Machine learning phases of matter. *Nature Physics*, 13(5):431–434, 2017.

[7] Shuo-Hui Li and Lei Wang. Neural network renormalization group. *Phys. Rev. Lett.*, 121:260601, 2018.

[8] Dian Wu, Lei Wang, and Pan Zhang. Solving statistical mechanics using variational autoregressive networks. *Phys. Rev. Lett.*, 122:080602, 2019.

[9] Giuseppe Carleo, Ignacio Cirac, Kyle Cranmer, Laurent Daudet, Maria Schuld, Naftali Tishby, Leslie Vogt-Maranto, and Lenka Zdeborová. Machine learning and the physical sciences. *Rev. Mod. Phys.*, 91:045002, 2019.

[10] Xinran Ma, Z. C. Tu, and Shi-Ju Ran. Deep learning quantum states for Hamiltonian estimation. *Chinese Physics Letters*, 38(11):110301, 2021.

[11] Tom Brown, Benjamin Mann, Nick Ryder, Melanie Subbiah, Jared D Kaplan, Prafulla Dhariwal, Arvind Neelakantan, Pranav Shyam, Girish Sastry, Amanda Askell, Sandhini Agarwal, Ariel Herbert-Voss, Gretchen Krueger, Tom Henighan, Rewon Child, Aditya Ramesh, Daniel Ziegler, Jeffrey Wu, Clemens Winter, Chris Hesse, Mark Chen, Eric Sigler, Mateusz Litwin, Scott Gray, Benjamin Chess, Jack Clark, Christopher Berner, Sam McCandlish, Alec Radford, Ilya Sutskever, and Dario Amodei. Language Models are Few-Shot Learners. In *Advances in Neural Information Processing Systems*, volume 33, pages 1877–1901. Curran Associates, Inc., 2020.

[12] Yann Le Cun, John S Denker, and Sara A Solla. Optimal brain damage. In *Proceedings of the 2nd International Conference on Neural Information Processing Systems*, pages 598–605, 1989.

[13] Zhuang Liu, Mingjie Sun, Tinghui Zhou, Gao Huang, and Trevor Darrell. Rethinking the value of network pruning. In *International Conference on Learning Representations*, 2019.

[14] Zi Wang, Chengcheng Li, and Xiangyang Wang. Convolutional neural network pruning with structural redundancy reduction. In *2021 IEEE/CVF Conference on Computer Vision and Pattern Recognition (CVPR)*, pages 14908–14917, 2021.

[15] Geoffrey Hinton, Oriol Vinyals, and Jeff Dean. Distilling the knowledge in a neural network. *Stat*, 1050:9, 2015.

[16] Jianping Gou, Baosheng Yu, Stephen J. Maybank, and Dacheng Tao. Knowledge distillation: A survey. *International Journal of Computer Vision*, 129(6):1789–1819, 2021.

[17] Steven J. Nowlan and Geoffrey E. Hinton. Simplifying neural networks by soft weight-sharing. *Neural Computation*, 4(4):473–493, 1992.

[18] Xiangxiang Chu, Bo Zhang, and Ruijun Xu. Fairnas: Rethinking evaluation fairness of weight sharing neural architecture search. In *2021 IEEE/CVF International Conference on Computer Vision (ICCV)*, pages 12219–12228, 2021.

[19] Kohei Hayashi, Taiki Yamaguchi, Yohei Sugawara, and Shinichi Maeda. Exploring unexplored tensor network decompositions for convolutional neural networks. In H. Wallach, H. Larochelle, A. Beygelzimer, F. d'Alché-Buc, E. Fox, and R. Garnett, editors, *Advances in Neural Information Processing Systems*, volume 32. Curran Associates, Inc., 2019.

[20] Ye Liu and Michael K. Ng. Deep neural network compression by tucker decomposition with nonlinear response. *Knowledge-Based Systems*, 241:108171, 2022.

[21] David Pérez-García, Frank Verstraete, Michael M. Wolf, and J. Ignacio Cirac. Matrix Product State Representations. *Quantum Inf. Comput.*, 7:401–430, 2007.

[22] C. Hubig, I. P. McCulloch, and U. Schollwöck. Generic construction of efficient matrix product operators. *Phys. Rev. B*, 95:035129, 2017.

[23] I. V. Oseledets. Tensor-train decomposition. *SIAM Journal on Scientific Computing*, 33(5):2295–2317, 2011.

[24] B Pirvu, V Murg, J I Cirac, and F Verstraete. Matrix product operator representations. *New Journal of Physics*, 12(2):025012, 2010.

[25] Alexander Novikov, Dmitrii Podoprikhin, Anton Osokin, and Dmitry P Vetrov. Tensorizing neural networks. In C. Cortes, N. Lawrence, D. Lee, M. Sugiyama, and R. Garnett, editors, *Advances in Neural Information Processing Systems*, volume 28. Curran Associates, Inc., 2015.

[26] Yong-Deok Kim, Eunhyeok Park, Sungjoo Yoo, Taelim Choi, Lu Yang, and Dongjun Shin. Compression of deep convolutional neural networks for fast and low power mobile applications. *arXiv preprint arXiv:1511.06530*, 2015.

[27] V. Aggarwal, W. Wang, B. Eriksson, Y. Sun, and W. Wang. Wide Compression: Tensor Ring Nets. In *2018 IEEE/CVF Conference on Computer Vision and Pattern Recognition (CVPR)*, pages 9329–9338, Los Alamitos, CA, USA, 2018.

[28] Ze-Feng Gao, Song Cheng, Rong-Qiang He, Z. Y. Xie, Hui-Hai Zhao, Zhong-Yi Lu, and Tao Xiang. Compressing deep neural networks by matrix product operators. *Phys. Rev. Res.*, 2:023300, 2020.

[29] Xingwei Sun, Ze-Feng Gao, Zhong-Yi Lu, Junfeng Li, and Yonghong Yan. A model compression method with matrix product operators for speech enhancement. *IEEE/ACM Transactions on Audio, Speech, and Language Processing*, 28:2837–2847, 2020.

[30] Shi-Ju Ran, Emanuele Tirrito, Cheng Peng, Xi Chen, Luca Tagliacozzo, Gang Su, and Maciej Lewenstein. *Tensor Network Contractions: Methods and Applications to Quantum Many-Body Systems*. Springer, Cham, 2020.

[31] Hai-Jun Liao, Jin-Guo Liu, Lei Wang, and Tao Xiang. Differentiable programming tensor networks. *Phys. Rev. X*, 9:031041, 2019.

[32] Peng-Fei Zhou, Rui Hong, and Shi-Ju Ran. Automatically differentiable quantum circuit for many-qubit state preparation. *Phys. Rev. A*, 104:042601, 2021.

[33] Y. Lecun, L. Bottou, Y. Bengio, and P. Haffner. Gradient-based learning applied to document recognition. *Proceedings of the IEEE*, 86(11):2278–2324, 1998.

[34] Karen Simonyan and Andrew Zisserman. Very deep convolutional networks for large-scale image recognition. *arXiv preprint arXiv:1409.1556*, 2014.

[35] http://yann.lecun.com/exdb/mnist.

[36] https://www.cs.toronto.edu/~kriz/cifar.html.

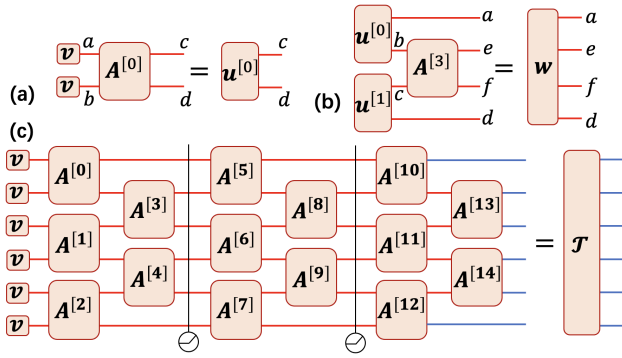**Appendix A: Basics of tensor network and the contractions**

FIG. 4. (Color online) In (a) and (b), we show the diagrammatic representations of two local contractions in the ADTN. The contraction of the whole ADTN results in a higher-order tensor $\mathcal{T}$ that stores the variational parameters of NN. The lowercase letters around the bonds indicate the indexes of tensors.

To explain how the higher-order tensor $\mathcal{T}$ by contracting the ADTN, we show in Fig. 4 (a) and (b) the diagrammatic representations of two local contractions as an example. As shown in (a), the contraction of one tensor $\boldsymbol{A}^{[0]}$ in ADTN and two vectors $\boldsymbol{v}$ reads

$$u^{[0]}_{cd} = \sum_{ab} v_a v_b A^{[0]}_{abcd}. \tag{A1}$$

Another example is the contraction shown in (b), which reads

$$w_{aefd} = \sum_{bc} u^{[0]}_{ab} u^{[1]}_{cd} A^{[3]}_{bcef}, \tag{A2}$$

where $\boldsymbol{u}^{[1]}$ can be the result of the contraction of $\boldsymbol{A}^{[1]}$ and two $\boldsymbol{v}$'s. Generally speaking, the contraction formulas and their diagrammatic representations are in one-to-one correspondence. After contracting all shared bonds (indexes) by following the same rules as Eqs. (A1) and (A2), the ADTN results in a higher-order tensor $\mathcal{T}$ that represents the variational parameters of NN, whose indexes are illustrated by the blue bonds in Fig. 4 (c).

With the presence of non-linear activations, the contractions should be done layer by layer, from left to right. After contracting one tensor layer, each element of the obtained tensor will be put into the activation function. In the simulations, we take the ReLU activation, where an element x is mapped as

$$\sigma(x) = \max(0, x). \tag{A3}$$

Appendix B: Details of FC-2, LeNet-5, AlexNet, AFNet and VGG-16

Below, we provide the structure and hyper-parameters of the NN's (FC2 in Table III, LeNet-5(MNIST) in Table IV,

LeNet-5 in Table V, AlexNet in Table VI, VGG-16 in Table VIII and reduced version VGG-16 in Table IX), for the convenience of reproducing our results.

TABLE III. Details of FC2.

Layer name	Input size	Paras	Output size
FC1	784	784×256	256
ReLU			
FC2	256	256×10	10

TABLE IV. Details of LeNet-5(MNIST).

Layer name	Input size	Paras	Output size
Conv1	$28 \times 28 \times 1$	[1;6;5;2]	$28 \times 28 \times 6$
ReLU			
MaxPool2	$28 \times 28 \times 6$		$14 \times 14 \times 6$
Conv2	$14 \times 14 \times 6$	[6;16;5;0]	$10 \times 10 \times 16$
ReLU			
MaxPool2	$10 \times 10 \times 16$		$5 \times 5 \times 16$
Conv3	$5 \times 5 \times 16$	[16;120;5;0]	$1 \times 1 \times 120$
FC1	120	120×84	84
ReLU			
FC2	84	84×10	10

TABLE V. Details of LeNet-5.

Layer name	Input size	Paras	Output size
Conv1	$32 \times 32 \times 3$	[3;16;5;1;0]	$28 \times 28 \times 16$
ReLU			
MaxPool2	$28 \times 28 \times 16$		$14 \times 14 \times 16$
Conv2	$14 \times 14 \times 16$	[16;32;5;1;0]	$10 \times 10 \times 32$
ReLU			
AdaptiveAvgPool2	$10 \times 10 \times 32$		$4 \times 4 \times 32$
FC1	512	512×256	256
ReLU			
FC2	256	256×128	128
ReLU			
FC3	128	$128 \times$class	class

TABLE VI. Details of AlexNet.

Layer name	Input size	Paras	Output size
Conv1	$32 \times 32 \times 3$	[3;64;3;2;1]	$16 \times 16 \times 64$
BatchNorm2d			
ReLU			
MaxPool2	$16 \times 16 \times 64$	[3;2]	$7 \times 7 \times 64$
SpConv2	$7 \times 7 \times 64$	[64;128;2;1;0]	$7 \times 7 \times 128$
BatchNorm2d			
ReLU			
MaxPool2	$7 \times 7 \times 128$	[3;2]	$3 \times 3 \times 128$
SpConv3	$3 \times 3 \times 128$	[128;256;2;1;0]	$3 \times 3 \times 256$
BatchNorm2d			
ReLU			
SpConv4	$3 \times 3 \times 256$	[256;512;2;1;0]	$3 \times 3 \times 512$
BatchNorm2d			
ReLU			
SpConv5	$3 \times 3 \times 512$	[512;512;2;1;0]	$3 \times 3 \times 512$
BatchNorm2d			
ReLU			
MaxPool2	$3 \times 3 \times 512$	[3;2]	$1 \times 1 \times 512$
Dropout(0.5)			
FC1	512	512×2048	2048
ReLU			
Dropout(0.5)			
FC2	2048	2048×2048	2048
ReLU			
FC3	2048	$2048 \times$class	class

TABLE VII. Details of ZFNet.

Layer name	Input size	Paras	Output size
Conv1	$32 \times 32 \times 3$	[3;64;3;2;1]	$16 \times 16 \times 64$
ReLU			
MaxPool2	$16 \times 16 \times 64$		$8 \times 8 \times 64$
SpConv2	$8 \times 8 \times 64$	[64;128;2;1;0]	$8 \times 8 \times 128$
ReLU			
MaxPool2	$8 \times 8 \times 128$	8	$4 \times 4 \times 128$
SpConv3	$4 \times 4 \times 128$	[128;128;2;1;0]	$4 \times 4 \times 128$
ReLU			
SpConv4	$4 \times 4 \times 128$	[128;256;2;1;0]	$4 \times 4 \times 256$
ReLU			
SpConv5	$4 \times 4 \times 256$	[256;256;2;1;0]	$4 \times 4 \times 256$
ReLU			
MaxPool2	$4 \times 4 \times 256$		$2 \times 2 \times 256$
Dropout(0.5)			
FC1	1024	1024×2048	2048
ReLU			
Dropout(0.5)			
FC2	2048	2048×2048	2048
ReLU			
Dropout(0.5)			
FC3	2048	$2048 \times$class	class

TABLE IX. Details of VGG-16(reduced version).

Layer name	Input size	Paras	Output size
Conv1	$32 \times 32 \times 3$	[3;64;2;1]	$32 \times 32 \times 64$
Conv2	$32 \times 32 \times 64$	[64;64;2;0]	$32 \times 32 \times 64$
ReLU			
MaxPool2	$32 \times 32 \times 64$		$16 \times 16 \times 64$
Conv3	$16 \times 16 \times 64$	[64;128;2;1]	$16 \times 16 \times 128$
Conv4	$16 \times 16 \times 128$	[128;128;2;0]	$16 \times 16 \times 128$
ReLU			
MaxPool2	$16 \times 16 \times 128$		$8 \times 8 \times 128$
Conv5	$8 \times 8 \times 128$	[128;256;2;1]	$8 \times 8 \times 256$
Conv6	$8 \times 8 \times 256$	[256;256;2;1]	$8 \times 8 \times 256$
ReLU			
Conv7	$8 \times 8 \times 256$	[256;256;2;0]	$8 \times 8 \times 256$
ReLU			
MaxPool2	$8 \times 8 \times 256$		$4 \times 4 \times 256$
Conv8	$4 \times 4 \times 256$	[256;512;2;1]	$4 \times 4 \times 512$
Conv9	$4 \times 4 \times 256$	[512;512;2;1]	$4 \times 4 \times 512$
ReLU			
Conv10	$4 \times 4 \times 256$	[512;512;2;0]	$4 \times 4 \times 512$
ReLU			
MaxPool2	$4 \times 4 \times 512$		$2 \times 2 \times 512$
Conv11	$2 \times 2 \times 512$	[512;1024;2;1]	$2 \times 2 \times 1024$
Conv12	$2 \times 2 \times 1024$	[1024;1024;2;1]	$2 \times 2 \times 1024$
ReLU			
Conv13	$2 \times 2 \times 1024$	[1024;1024;2;0]	$2 \times 2 \times 1024$
ReLU			
MaxPool2	$2 \times 2 \times 1024$		$1 \times 1 \times 1024$
Dropout(0.8)			
FC1	1024	1024×512	512
ReLU			
Dropout(0.8)			
FC2	512	512×256	256
ReLU			
Dropout(0.8)			
FC3	256	256×10	10

TABLE VIII. Details of VGG-16.

Layer name	Input size	Paras	Output size
Conv1	$32 \times 32 \times 3$	[3;96;3;1;1]	$32 \times 32 \times 96$
		BatchNorm2d	
		ReLU	
Conv2	$32 \times 32 \times 96$	[96;96;3;1;1]	$32 \times 32 \times 96$
		BatchNorm2d	
		ReLU	
MaxPool2	$32 \times 32 \times 96$	[2;2]	$16 \times 16 \times 96$
Conv3	$16 \times 16 \times 96$	[96;128;3;1;1]	$16 \times 16 \times 128$
		BatchNorm2d	
		ReLU	
Conv4	$16 \times 16 \times 128$	[128;128;3;1;1]	$16 \times 16 \times 128$
		BatchNorm2d	
		ReLU	
MaxPool2	$16 \times 16 \times 128$	[2;2]	$8 \times 8 \times 128$
Conv5	$8 \times 8 \times 128$	[128;256;3;1;1]	$8 \times 8 \times 256$
		BatchNorm2d	
		ReLU	
Conv6	$8 \times 8 \times 256$	[256;256;3;1;1]	$8 \times 8 \times 256$
		BatchNorm2d	
		ReLU	
Conv7	$8 \times 8 \times 256$	[256;256;3;1;1]	$8 \times 8 \times 256$
		BatchNorm2d	
		ReLU	
MaxPool2	$8 \times 8 \times 256$	[2;2]	$4 \times 4 \times 256$
Conv8	$4 \times 4 \times 256$	[256;512;3;1;1]	$4 \times 4 \times 512$
		BatchNorm2d	
		ReLU	
Conv9	$4 \times 4 \times 512$	[512;512;3;1;1]	$4 \times 4 \times 512$
		BatchNorm2d	
		ReLU	
Conv10	$4 \times 4 \times 512$	[512;512;3;1;1]	$4 \times 4 \times 512$
		BatchNorm2d	
		ReLU	
MaxPool2	$4 \times 4 \times 512$	[2;2]	$2 \times 2 \times 512$
Conv11	$2 \times 2 \times 512$	[512;512;3;1;1]	$2 \times 2 \times 512$
		BatchNorm2d	
		ReLU	
Conv12	$2 \times 2 \times 512$	[512;512;3;1;1]	$2 \times 2 \times 512$
		BatchNorm2d	
		ReLU	
Conv13	$2 \times 2 \times 512$	[512;512;3;1;1]	$2 \times 2 \times 512$
		BatchNorm2d	
		ReLU	
MaxPool2	$2 \times 2 \times 512$	[2;2]	$1 \times 1 \times 512$
FC1	512	512×4096	4096
		ReLU	
		Dropout(0.4)	
FC2	4096	4096×4096	4096
		ReLU	
		Dropout(0.4)	
FC3	4096	$4096 \times$class	class